Fermi National Accelerator Laboratory

FERMILAB-FN-565

Radiation Damage, Calibration and Depth Segmentation in Calorimeters

D. Green and A. Para

Fermi National Accelerator Laboratory
P.O. Box 500
Batavia, Illinois 60510

May 1991

Operated by Universities Research Association Inc. under contract with the United States Department of Energy

FN565
May 1991

RADIATION DAMAGE, CALIBRATION AND DEPTH SEGMENTATION IN CALORIMETERS

Dan Green and Adam Para
Fermi National Accelerator Laboratory
Batavia, Illinois 60510*

John Hauptman
Iowa State University
Ames, Iowa 50011

1. INTRODUCTION

The advent of the SSC will make severe demands on calorimetry. In particular, the radiation field is formidable. For example, the dose at *EM* shower maximum due to interactions alone for a luminosity of $10^{34}/cm^2sec$ for a 10 year (1 year = 10^7 sec) lifetime is up to 50 Mrad.[1] Given the severity of the problem, we have herein attempted to evaluate methods to alleviate the damage using a combination of calibration and correction on an event by event basis using the presumed longitudinal segmentation of the *EM* calorimetry.

2. SIMPLE ESTIMATIONS

2.1 Conversion Point Fluctuations

A simple minded model was first made in order to get an intuition about the physical processes in question. The basic assumption is that the *EM* shower has many particles in it, so that the main fluctuation is in the conversion point t (in radiation length units) and not in the shower shape. Expressing the energy, E, in critical energy units, $y = E/Ec$, one takes a shower shape of;[2]

$$\frac{(dE/dbt)}{E} = \left[(bt)^{a-1}\, exp(-bt)\right] / \Gamma(a), \qquad (1)$$

where $b \sim 0.5$ for iron, and $a = 1 + b\,[ln(y) - 0.5]$. The damage profile due to the radiation dose is taken to be a Gaussian with "depth" of damage parametrized by d and width parametrized by the standard deviation of the Gaussian.

$$f(t) = 1 - d\left\{exp\left[-(t-t_0)^2/2\sigma^2\right]\right\}. \qquad (2)$$

The damage peaks at a mean depth t_0 which characterizes the minimum bias events, with $E = p_T/sin(\theta)$. At rapidity = 3, this is $E \sim 6\ GeV$, or $t_0 \sim 6$.[3] The width can be estimated from shower profile curves,[3] to be $\sigma \sim 2.5$. This shower shape, with

a variable conversion point, is convoluted with the damaged calorimeter characterized by $f(t)$. For $d=0$, one obtains the integral of Eq. 1 = E by definition, independent of the conversion point t. Note that the characteristic scale of conversion point fluctuations is given by the radiation length itself or $dt \sim 1$.

2.2 Nonlinearities

For a non-zero d, the calorimeter is effectively a non-uniform medium. Thus, the fluctuation in the conversion point causes a fluctuation in the measured energy, which is the integral of $dE \cdot f(t)$. These fluctuations cause a degraded energy resolution, $dE = E_{meas} - E$. Note also that, as the energy increases the shower maximum extends logarithmically deeper into the calorimeter, and since it moves away from the damaged region, the measured energy is now a nonlinear function of the incident energy. For example, a 1 TeV electron has a shower maximum at a depth of ~ 11.5 radiation lengths, which is ~ 2 standard deviations away from the damaged region located at ~ 6 radiation lengths.

The fractional shift, dE/E, in the energy as a function of energy is shown in Fig. 1 for different damage parameters. Also shown is the region dominated by the calorimeter resolution, taken to be $dE/E = 0.2/\sqrt{(E)} \oplus 0.01$, and not the damage. Clearly for $d > 0.1$, the nonlinearity due to damage exceeds the undamaged resolution. One also notes that the shift increases with damage, as expected. In addition, the shift decreases with energy, which reflects the fact that the location of shower maximum increases with E. The curves are an eyeball fit to the points;

$$dE/E = d[g + h \cdot \ell n(E)] \tag{3}$$

Given the shape defined in Eq. 1, a logarithmic energy dependence is not surprising. The shift appears adequately described as linear in the damage parameter. The fractional shift as a function of d is shown in Fig. 2. For any fixed conversion point, t, the shift is linear in d. At fixed energy, the shift is also linear in t, with larger t leading to reduced shift. This is clearly an effect of moving away from the damage region, and thus experiencing a lesser loss of response. A rough parametrization of the shift is;

$$dE/E = d[g + h \cdot \ell n(E)] \cdot (1 - m \cdot t) \tag{4}$$

For $d = 0.5$, a fluctuation in t of $dt = \pm 1$, leads to an energy fluctuation of $\pm 4\%$ at an energy of 100 GeV. Since this far exceeds the "constant term" of most high quality calorimeters, the shift must be corrected for if performance is not to be seriously compromised. The size of an acceptable 1% constant term is shown as the shaded region in Fig. 2 in order to set the scale.

2.3 Depth Segmentation Ratio

Clearly, one needs some measure of the conversion point in order to make a correction. First, one imagines adopting a source tube[4] deployed longitudinally, such

that d, t_{σ} and σ may be continuously measured and monitored. Then, using Eq. 4, if t is known, and E is estimated (it is only a soft logarithmic dependence), one can correct by dE on an event by event basis.

The estimate for t comes from the assumed depth segmentation. The quantity which is used is the ratio, R, of energy in the first 10 radiation lengths, to the total energy in 40 t, $R \equiv E(0,10)/E(0,40)$. In Fig. 4 is shown the ratio R as a function of energy for shower initiation points of $t = 0, 1, and\ 2$. Points are shown for $d=0$ and $d=0.5$. The curves are a simple parametrization;

$$R = [1 - r \bullet d + s \bullet d / \ell n(E)][u - v \bullet \ell n(E)](1 - w \bullet t). \qquad (5)$$

The main point is that R depends on t, and decreases with increasing t, as expected since larger t means deeper into the calorimeter, and hence reduced R. As d increases, R decreases, since the front region of the calorimeter is deadened. Finally, R decreases as E increases, again since larger E emphasizes the rear of the calorimeter.

Using Eq. 5, the energy is corrected for. Even with the rough representations of the data points, one obtains a corrected energy for $d < 0.5$, $E > 30\ GeV$, and $t < 2$, with accuracy better than 1%. This success leads one to continue the study at a more quantitative level, including the damage profile $f(t)$ in a more accurate fashion, and including the fluctuations in the EM shower itself. This Monte Carlo approach is pursued in Section 3.

Using Eq. 4 and Eq. 5, one may estimate the required accuracy of the measurements of the damage profile $f(t)$ and the ratio R which is needed to preserve the resolution of the EM calorimetry. The energy itself contributes logarithmically, so its accuracy is assumed to be sufficient. The shift depends linearly on d, so that the calibration procedure must supply d to some accuracy. For $E > 100\ GeV$, or $p_T > 10\ GeV$ at $y=3$, the error in dE/E is ~ 0.3 times the error in d. For the worst case of $d=0.5$, a determination of d to 10% means an error on dE/E of $< 1.5\%$, which is acceptable.

Using Eq. 5, if R is measured in each event, then t is inferred. The dependence of R on E and d is soft, as seen in Fig. 3. For $E > 100\ GeV$, and $d=0.5$, the error on dE/E is < 0.037 times the error on t. The error on R is, in turn, 0.065 times the error on t. If the energy, E, is measured to 2%, then the error on the ratio, R, is 1%, which means t is measured to, $dt \sim 0.16$. Given the dependence shown in Eq. 4, the correction to energy is good to $< 0.6\%$, which is again sufficient.

2.4 Damage Profile Dependence

The error analysis done above has been for a fixed Gaussian damage profile, $f(t)$, with a standard deviation of 2.5. It is also important to investigate the sensitivity of the results to profile variations. In Fig. 4. is shown the dependence of the energy shift on the assumed shape of the damage profile. Three cases were examined, $\sigma=2.5$, $\sigma=3.5$, and a Lorentzian with full width such that the standard deviation was = 2.5.

In Fig. 4a. is plotted the fractional shift as a function of energy with fixed damage, $d=0.5$, and fixed conversion point, $t=0$. Clearly the two Gaussians lead one to parametrize as;

$$dE/E = d[g + h \cdot \ln(E) + j \cdot \sigma] \cdot (1 - m \cdot t). \quad (6)$$

A larger σ means that the damage spreads over a larger fraction of the calorimeter, leading to an increased shift at all energies. Comparing the Gaussian and the Lorentzian, the longer tails in the latter case lead to a larger shift and a slope with energy which is softer. The reasons for this behavior are physically obvious. The points in Fig. 4b. are the energy shift as a function of t at fixed energy, $E = 100$ GeV, for $d=0.5$, and for the 3 cases. The slope m appears to be shape independent to a sufficient accuracy.

The dependence of the ratio R on shape parameters was also looked at. This quantity is only very weakly dependent on shape for the 3 cases herein considered. Hence, the estimates of the required accuracy on R are probably stable with respect to the exact shape of the damage profile. The numerical relation between the error on d and that on energy are shape dependent, as seen in Eq. 6. More detailed studies require a complete Monte Carlo analysis.

3. EGS STUDIES

3.1. Calorimeter Simulation, Radiation Damage Model.

The calorimeter was assumed to consist of 5 mm lead plates alternating with 3 mm polystyrene scintillator tiles. Electron-induced showers of 1, 5, 10, 20, 50, and 100 GeV energy were simulated with the EGS4 code, and energy depositions in each individual plane were stored. The low-energy cutoff for electrons and photons was set to 100 keV.

Radiation damage effects were simulated assuming that the amount of light collected from a given plane is reduced by a factor proportional to the integrated energy deposition in this plane due to the minimum bias events. All the radiation damage is assumed to be due to photons from π^0's produced in minimum bias interactions. Their energy will vary with polar angle from about 0.6 GeV at $90°$ $(y=0)$ to 6.0 GeV at $(y=3)$. In this study we have used 1 GeV electron showers as a damaging agent. Energy (light) registered at a given depth in the calorimeter will be reduced by an amount proportional to the profile, $g(t)$, of a 1 GeV electron shower:

$$E_{meas}(t) = E(t) \cdot [1 - d \cdot g(t)] \quad (7)$$

$E(t)$ is the energy observed with a 'non-damaged' calorimeter at a given depth t. $E_{meas}(t)$ is the energy observed at this depth with a damaged calorimeter. The function $g(t)$ is the longitudinal profile of the damage, assumed to correspond to the average shower profile of 1 GeV electrons. The damage parameter d is the measure of the damage; $d=1$ corresponds to a situation where the detector is dead, at shower max.

3.2 Effects of the Radiation Damage on the Detector Performance, Case 1 Unitary *EM* Calorimeter

Figure 5 shows the observed energy distributions for 50 GeV electrons, for 3 cases: $d=0$ (i.e. no damage), $d=0.5$ and $d=1.0$. As expected, the observed energy distribution shifts towards small pulse heights as d increases. At the same time, the relative width increases, indicating an additional contribution to the energy resolution. Fig. 6 shows the drop of the mean observed pulse height, the resolution (taken as RMS of the pulse height distribution), and the contribution of the radiation damage to the energy resolution (defined as the quadratic difference of the resolution after and before the damage) as a function of the damage parameter d, for 100 GeV electrons.

Given the fact that the shape of the shower profile changes slowly with energy, whereas the damage profile is fixed, the radiation damage effects (change of response, and of resolution) will depend on the energy of the electron (photon) in question. Fig. 7 shows the induced non-linearity of the electromagnetic calorimeter (i.e., ratio of the observed response to that of the perfect detector) for three values of d equal to 0.1, 0.3 and 0.5. The induced non-linearity in an energy range from 1 to 100 GeV varies from 2% at $d=0.1$ *to* 13% *at* $d=0.5$.

Figure 8 shows the radiation damage induced additional contribution to the energy resolution for the same peak damage, d. This is not a "constant term"; it decreases logarithmically with energy in the range from 1 to 100 GeV. This Fig. shows that if one does not measure/correct for the radiation-induced resolution effect, then the amount of damage must be kept below $d=0.3$. The same conclusion was reached for a uranium-scintillator calorimeter, using the GEANT 4 simulation package, as shown in Fig. 9.

3.3 Effects of Radiation Damage on Detector Performance, Case 2 - Depth-Segmented *EM* Calorimeter

As shown in Section 2, the dominant contribution to the additional resolution effects are due to fluctuations in the position of the first conversion. Showers which start later develop in a less damaged part of the detector and therefore produce more light. This results in the high-energy tail of the pulse height distribution seen in Fig. 5. One can attempt to measure this effect by sub-dividing the *EM* calorimeter into two sections, the first 10 t, and the rest. The fraction of the pulse height of a shower observed in the first section is strongly correlated with the position of the shower initiation, and hence can be used to correct the observed pulse height.

Figure 10 shows the scatter plot of the observed pulse height in the calorimeter vs. the fraction of the pulse height observed in the first 10 t for 50 GeV electrons, and $d=1$. As expected, events with relatively small energy deposit in the front section have larger observed energy than those which develop early in the calorimeter. Using a linear parametrization of the observed energy as a function of the fraction of the energy in the first section, one can correct the observed pulse height. In what follows, no dependence on d or E was assumed. Clearly, from Eq. 5, this procedure is not optimal but serves to indicate possibilities.

Figure 11 shows the result of a fit to the mean observed energy as a function of the fraction of energy in the front section, for 50 GeV electrons and $d=1$. These parametrizations can be used subsequently to correct the observed pulse height on an

event-by-event basis, depending on the fraction of the energy measured in the first *EM* section. Such a procedure will substantially reduce the non-linearity of the calorimeter, as shown in Fig. 12.

Even for the severe case of $d=0.5$, the non-linearity is of the order of 4% in the 1 to 100 GeV range. At the same time, the resolution of the calorimeter is also greatly improved. The radiation damage induced contribution to the resolution is below 2% for the energy range 10 to 100 GeV, for $d=0.5$ (see Fig. 13). We take this to be sufficient proof that the effects of radiation damage can be removed (on the scale of the baseline *EM* resolution) by this procedure. It was not felt necessary to refine the parametrization of Fig. 11 further. It should be stressed, however, that this correction scheme will only work for an isolated electron/photon. Any correction will be very difficult for electrons near hadronic jets, and totally impossible for the measurement of jet energy. Radiation damage to the electromagnetic calorimeter will result in a degradation of the energy resolution for hadronic jets. The dominant effect is due to the reduced response to the electromagnetic component of the jet. For $d=0.5$, the radiation damage was found to reduce the observed average jet energy by ~ 6%. Fluctuations in the π^0 content then lead to an additional contribution to the energy resolution of the order of 4%.

4. SUMMARY AND CONCLUSIONS

The effects of radiation damage in *EM* calorimetry were studied. First a simple model with a fixed shower shape and a fluctuating conversion point was used. The relations between damage profile $f(t)$, energy shift dE, and conversion point fluctuation t were examined. A longitudinal segmentation of the *EM* calorimeter was employed which would provide an event by event measurement of t. Given t and the damage profile $f(t)$, one can correct the energy E. One will monitor $f(t)$ continuously using movable radioactive sources.

The simple model was expanded to include a more realistic damage profile and to include the effects of fluctuations in the shower profile. The expectations of the simple model were confirmed. With the simplest d and E independent linear fit to the longitudinal energy ratio the residual non-linearity is small, and the calorimeter resolution term due to damage is less than 2% for damage parameter $d < 0.5$. Without a correction the energy resolution is degraded by an additional constant term of size 3.5% for $d = 0.5$. For jets one cannot make the correction.

4. REFERENCES

[1]Letter of Intent by the Solenoidal Detector Collaboration, November 30, 1990, SDC-90-00151.
[2]Review of Particle Properties, Physics Lett. **B239**, 1-516 (1990).
[3]D. Muller, Phys. Rev. **D5**, 2677 (1972).
[4]V.E. Barnes and A.T. Laasanen, ICCHEP Presentation, October 29-November 1, 1990, Fermilab.

5. FIGURE CAPTIONS

Fig. 1. Fractional shift in the mean energy as a function of electron energy for damage parameters $d=0.1$, •, $d=0.3$, O, and $d=0.5$, ⊕. The shaded region corresponds to a resolution dE/E of $0.2/\sqrt{(E)} \oplus 0.01$. A conversion point $t=0$ has been used. The lines are a function described in the text.

Fig. 2. Fractional shift in the mean energy as a function of damage parameter d. The shaded region corresponds to the size of the "constant term," $dE/E = 0.01$. The energy of the electron is fixed at $E=100$ GeV. The points are for conversion points $t=0$, •, $t=1$, O, and $t=2$, ⊕.

Fig. 3. Ratio of energy deposited in the first 10 radiation lengths to the energy deposited in 40 radiation lengths as a function of electron energy. The points correspond to conversion points at $t=0$, •, $t=1.0$, O, and $t=2.0$, ⊕. The curves correspond to a functional form described in the text.

a. damage parameter = 0.0
b. damage parameter = 0.5.

Fig. 4. Fractional energy shifts for different damage profile shapes. The points refer to a Gaussian with standard deviation in t of 2.5, •, and 3.5, 0, and a Lorentzian with full width such as to have the same standard deviation = 2.5, x. The curves correspond to functions described in the text.

a. Damage parameter = 0.5, and conversion point $t=0.0$. Shift as a function of energy.

b. Energy = 100 GeV and damage parameter 0.5. Shift as a function of conversion point.

Fig. 5. Observed energy distribution of 50 GeV electrons for damage parameter $d=0$, *solid line*, 0.5, *dotted line*, and 1.0, *dashed line*.

Fig. 6.a. Mean observed energy as a function of damage parameter.

b. Resolution for 100 GeV electrons as a function of damage parameter

c. Radiation-damage-induced contribution to the resolution as a function of damage parameter.

Fig. 7. Non-linearity of the electromagnetic calorimeter for damage parameter 0.1, 0.3 and 0.5.

Fig. 8. Additional contribution to the resolution as a function of the electron energy for damage parameter $d=0.1$, 0.3, and 0.5.

Fig. 9. Additional contribution to the energy resolution for *100 GeV* electrons in uranium-scintillator calorimeter as a function of damage parameter.

Fig. 10. Observed energy vs. ratio of energy deposited in the first 10 radiation lengths to the energy deposited in 40 radiation lengths for *50 GeV* electrons and damage parameter *d=1.*

Fig. 11. Mean observed energy as a function of a ratio of energy deposited in first *10 t* to the total shower energy. The line is a straight line fit to this distribution.

Fig. 12. Non-linearity of the electromagnetic calorimeter after correction for the radiation damage effects for damage parameter *0.1,* □, *0.3,* ○, *0.5,* and △.

Fig. 13. Contribution the the energy resolution of the electromagnetic calorimeter, after correction for the radiation damage, for damage parameter *0.1, 0.3, and 0.5.*

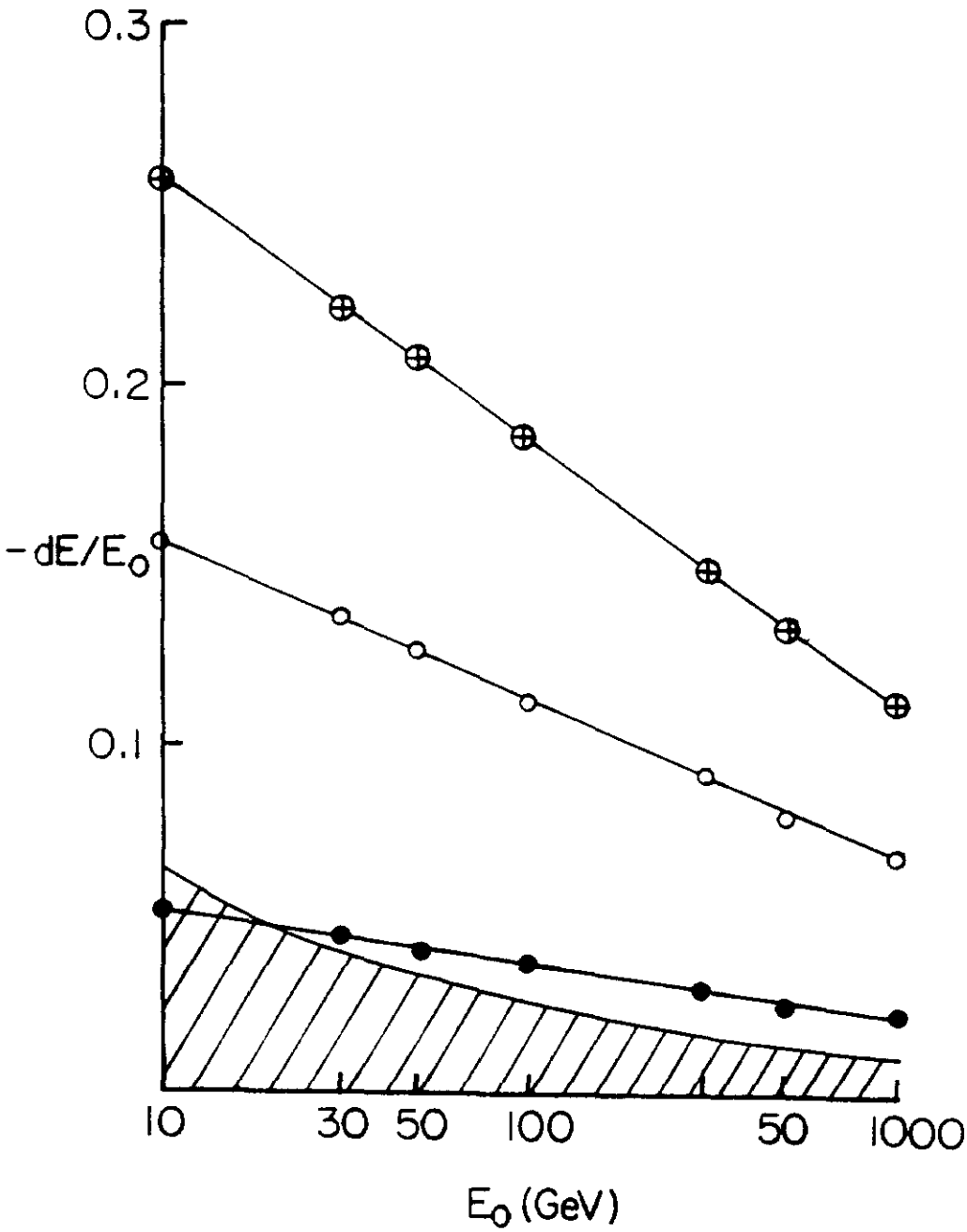

Figure 1.

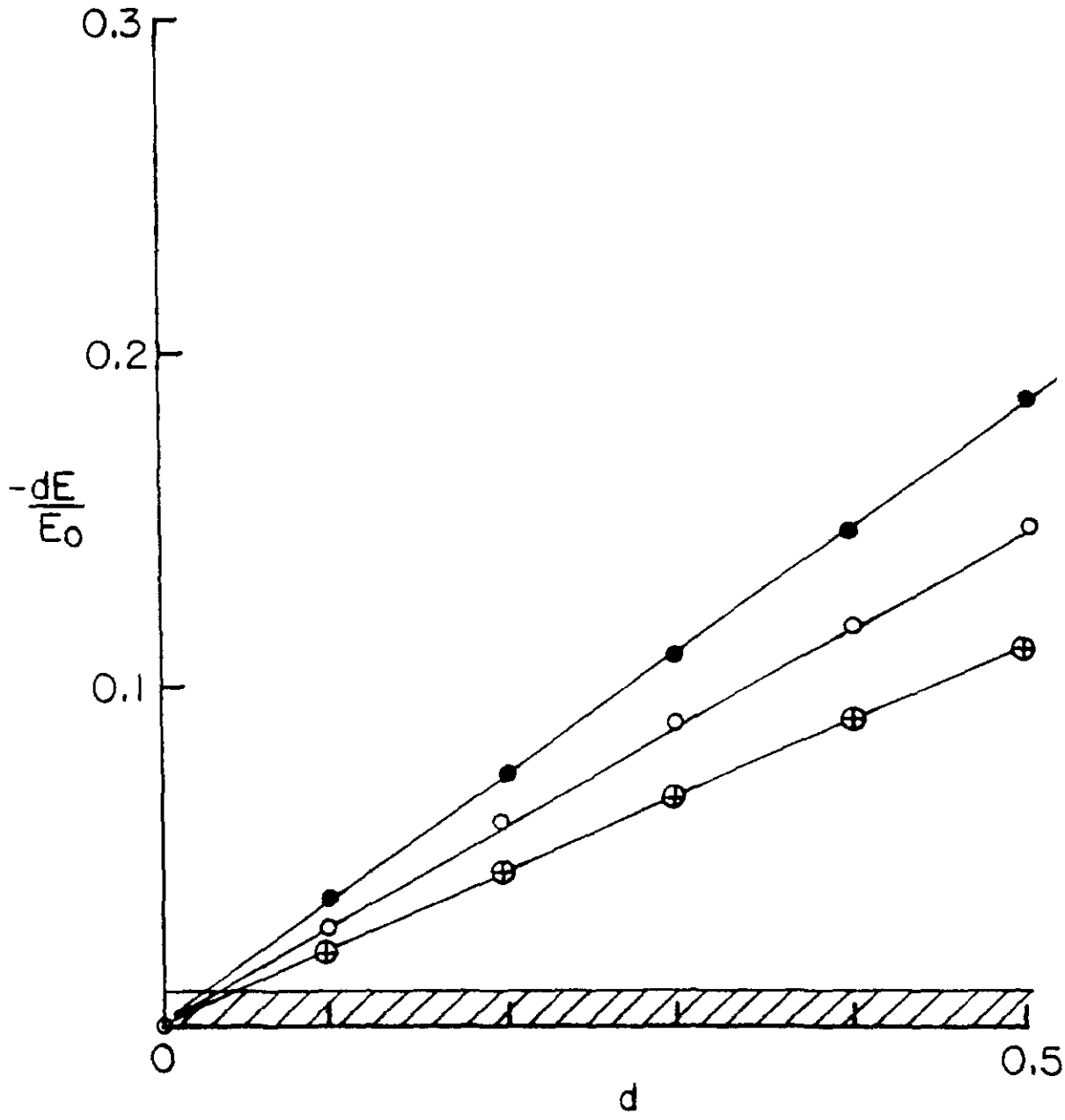

Figure 2.

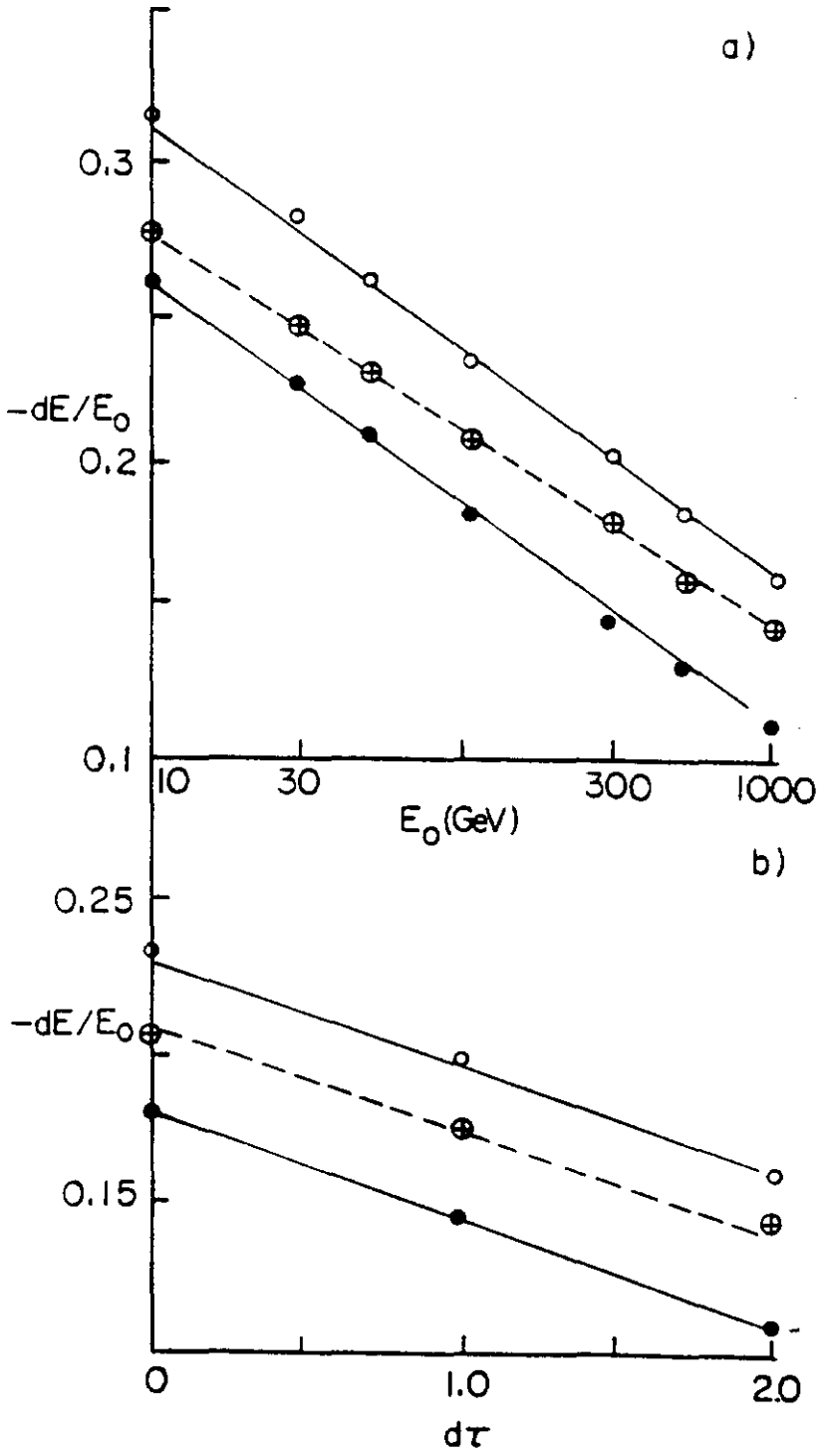

Figure 4.

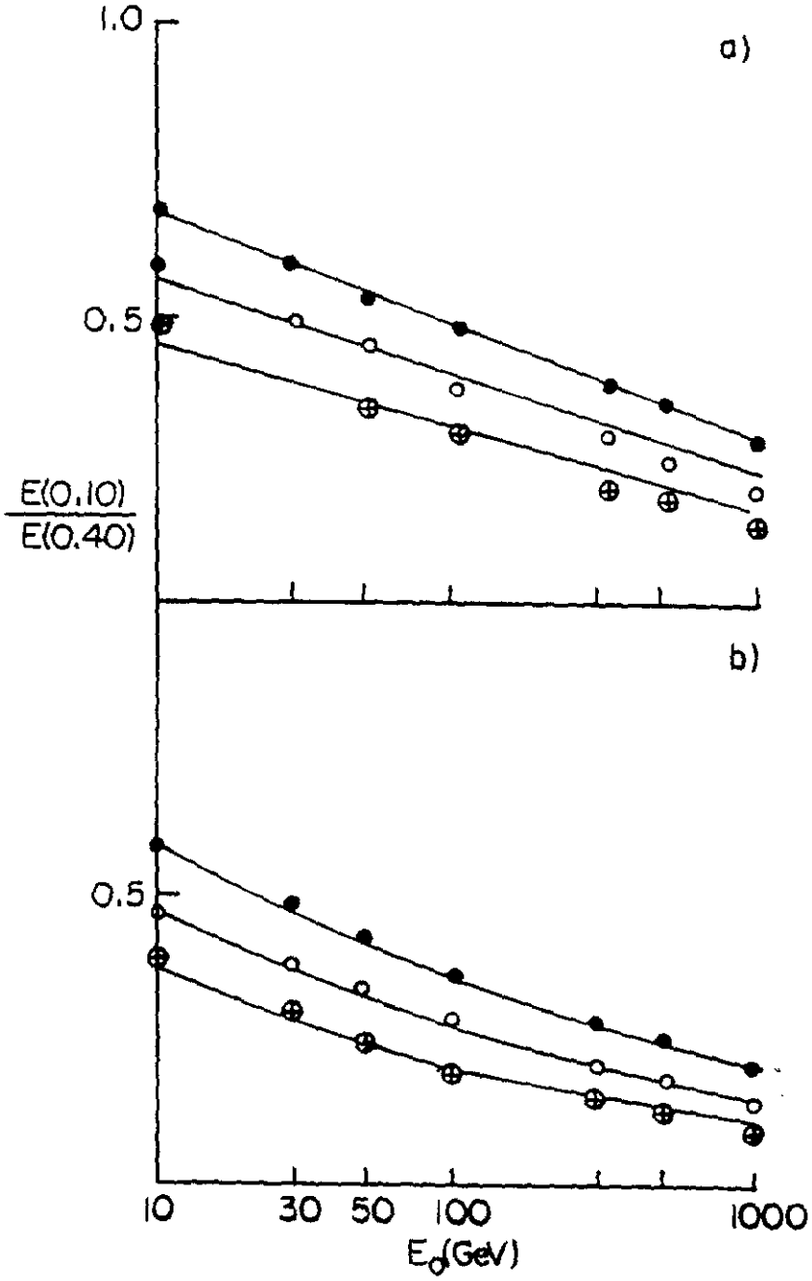

Figure 3.

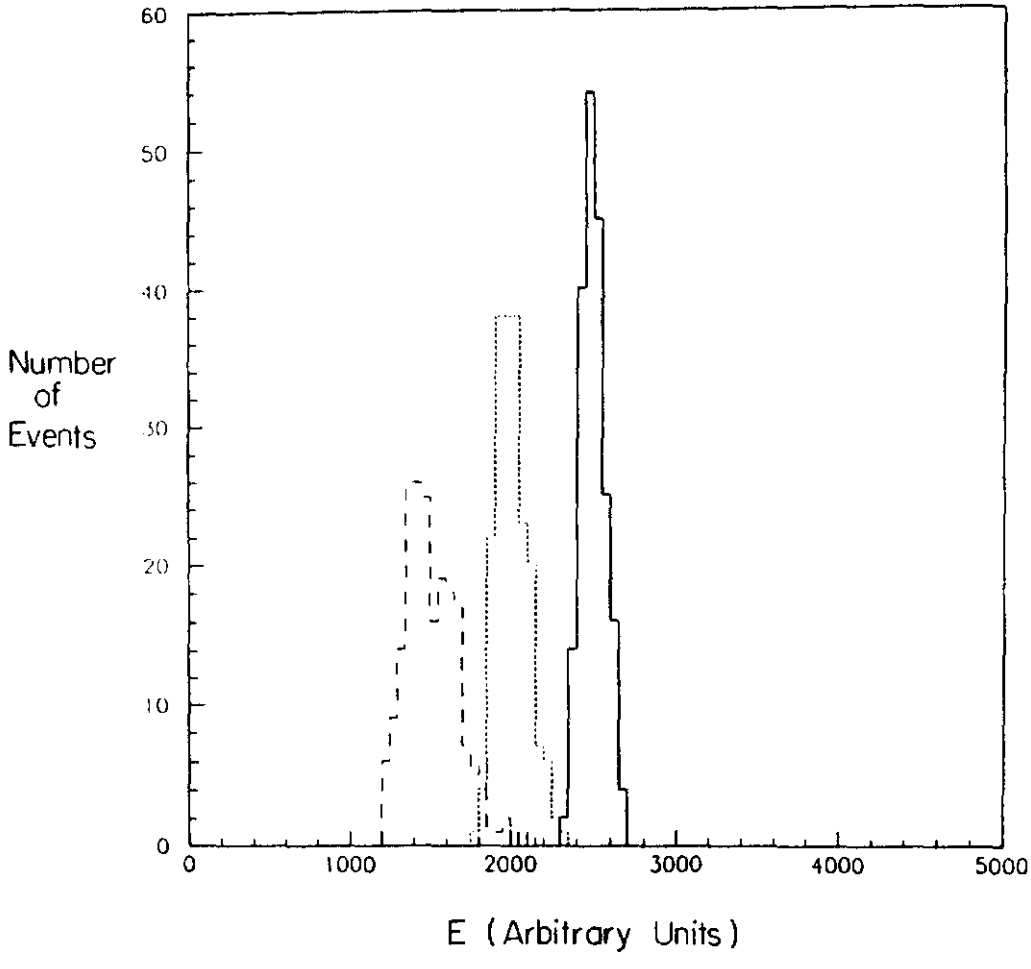
60
50
40
30
20
10
0
Number
of
Events
0
1000
2000
3000
4000
5000
E (Arbitrary Units)

Figure 5.

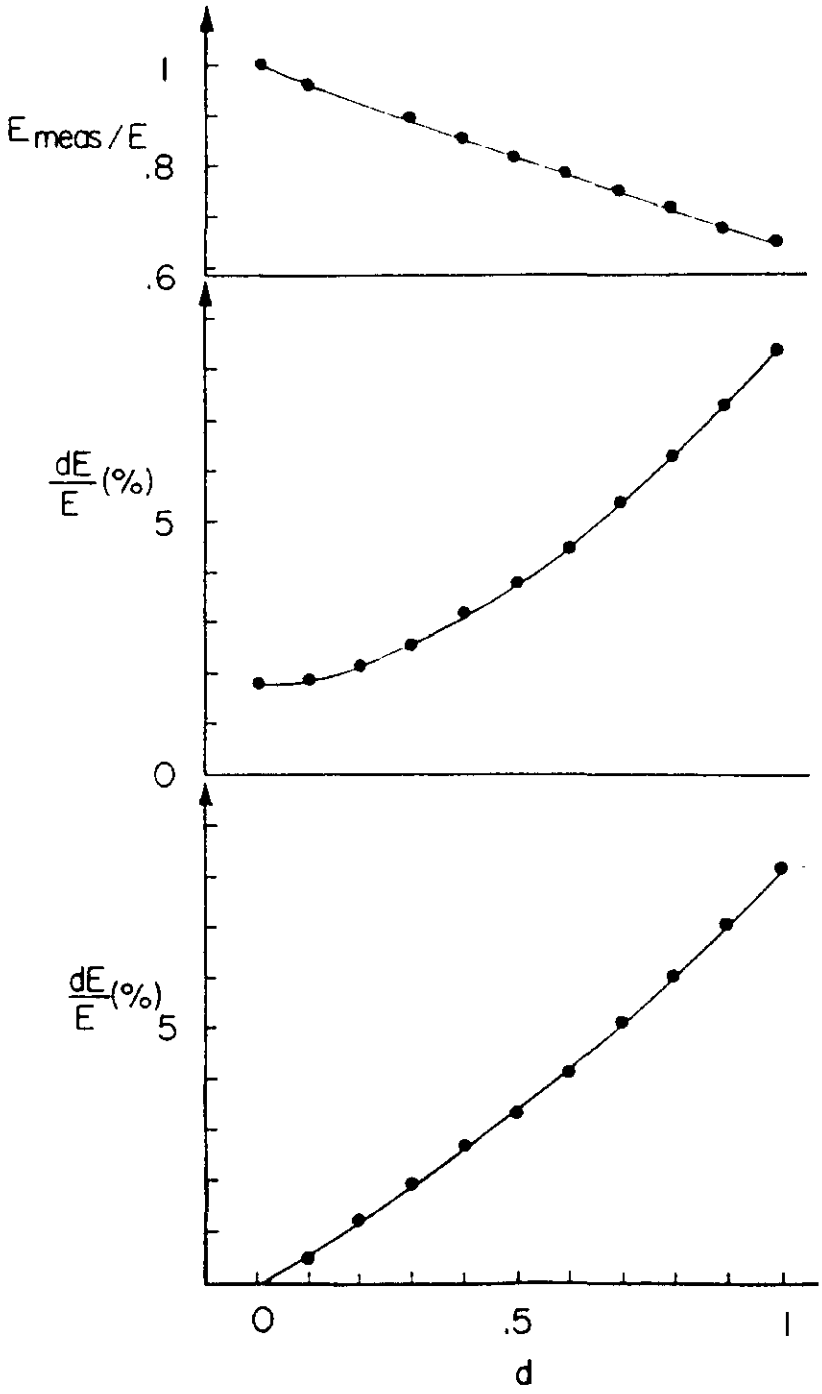

Figure 6.

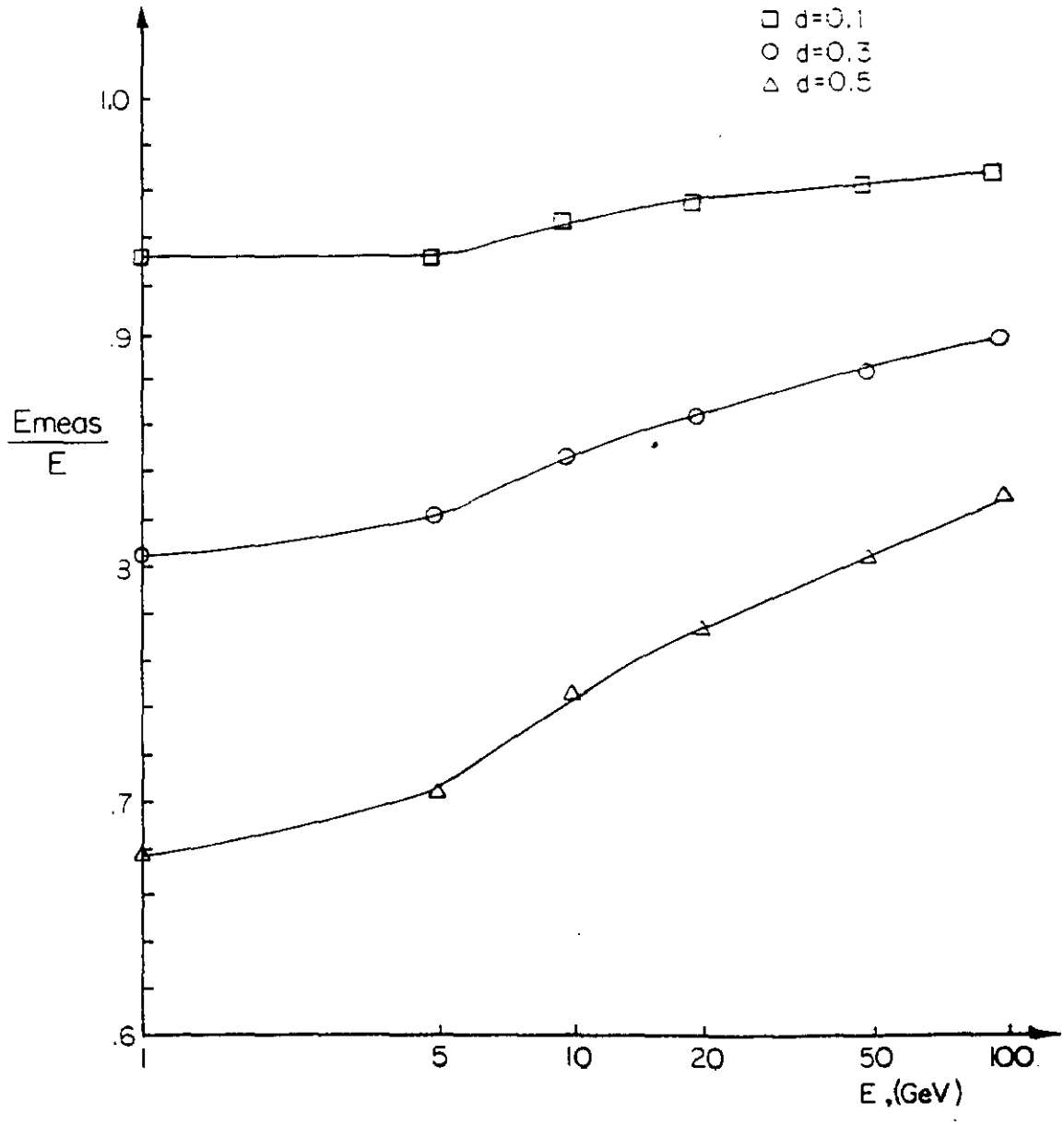

Figure 7.

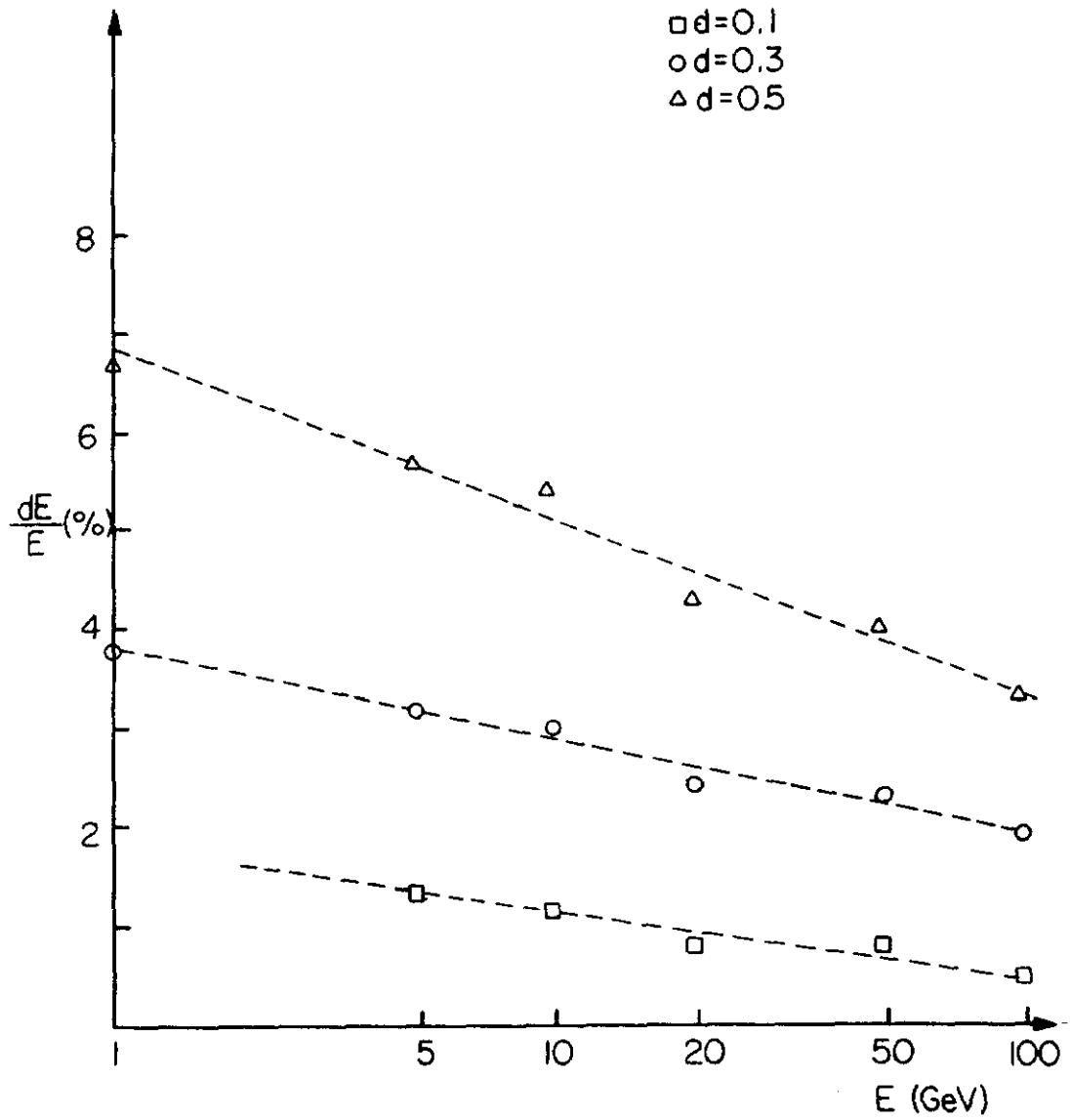

Figure 8.

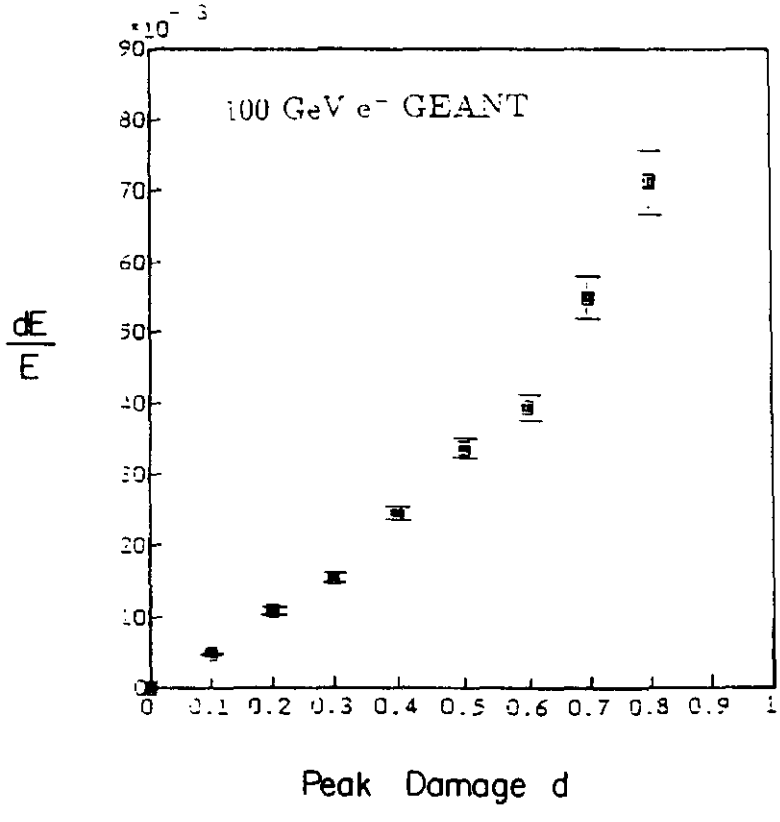

Figure 9.

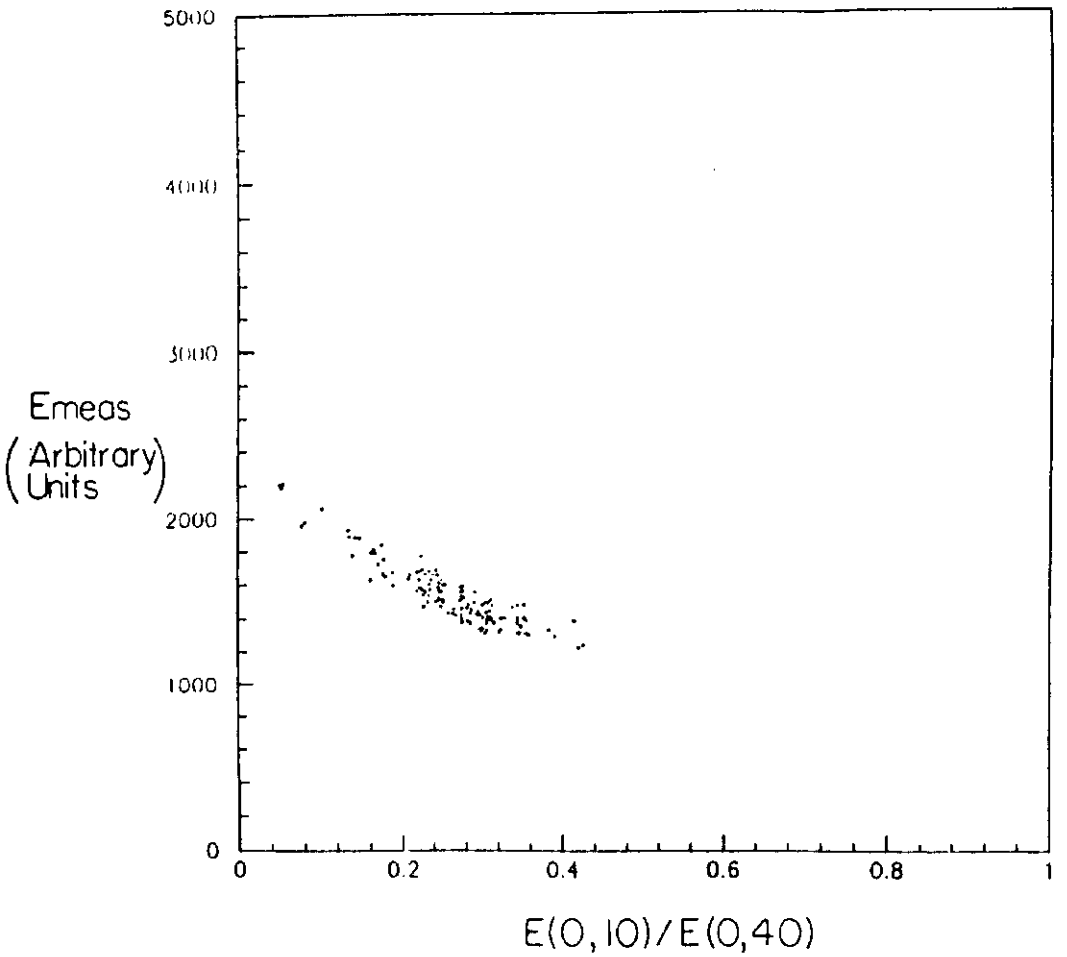
5000
4000
3000
2000
1000
0
Emeas
(Arbitrary Units)
0
0.2
0.4
0.6
0.8
1
E(0,10)/E(0,40)

Figure 10.

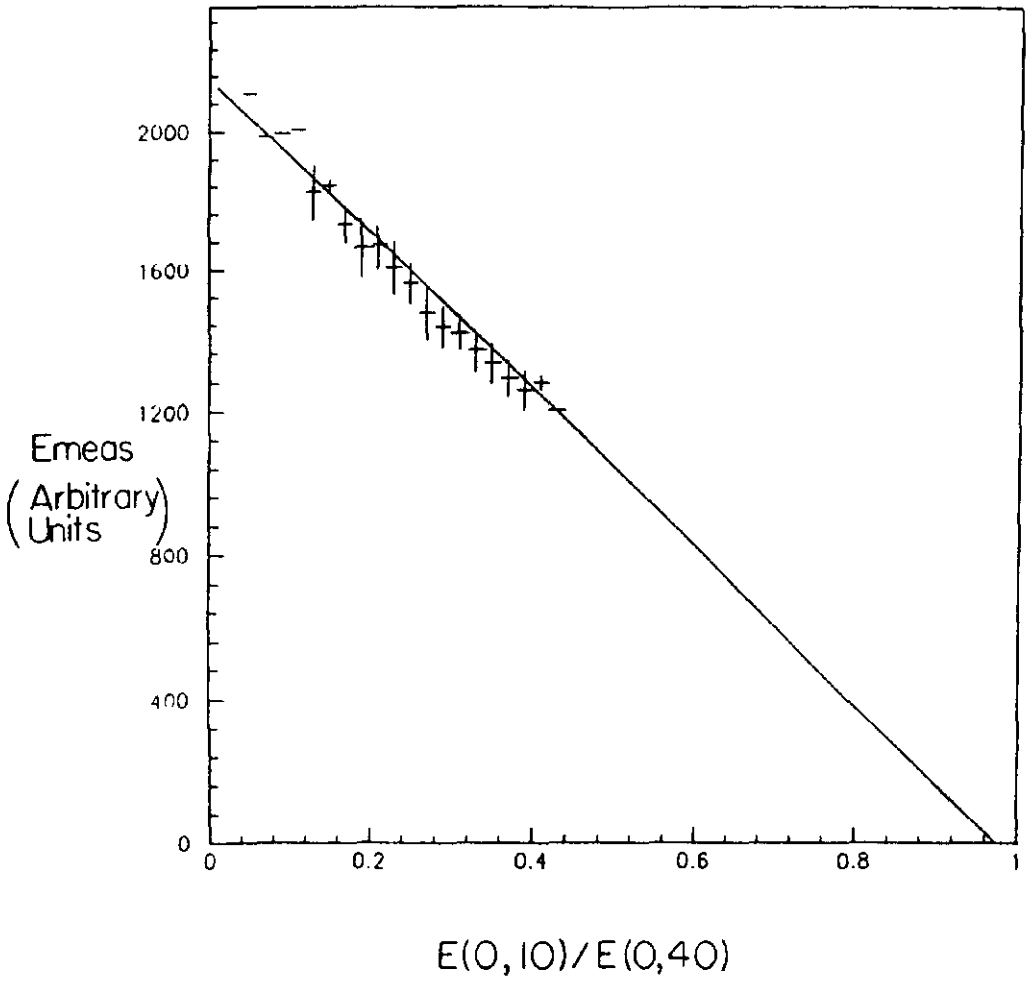
2000
1600
1200
800
400
0
Emeas
(Arbitrary Units)
0
0.2
0.4
0.6
0.8
1
E(0,10)/E(0,40)

Figure 11.

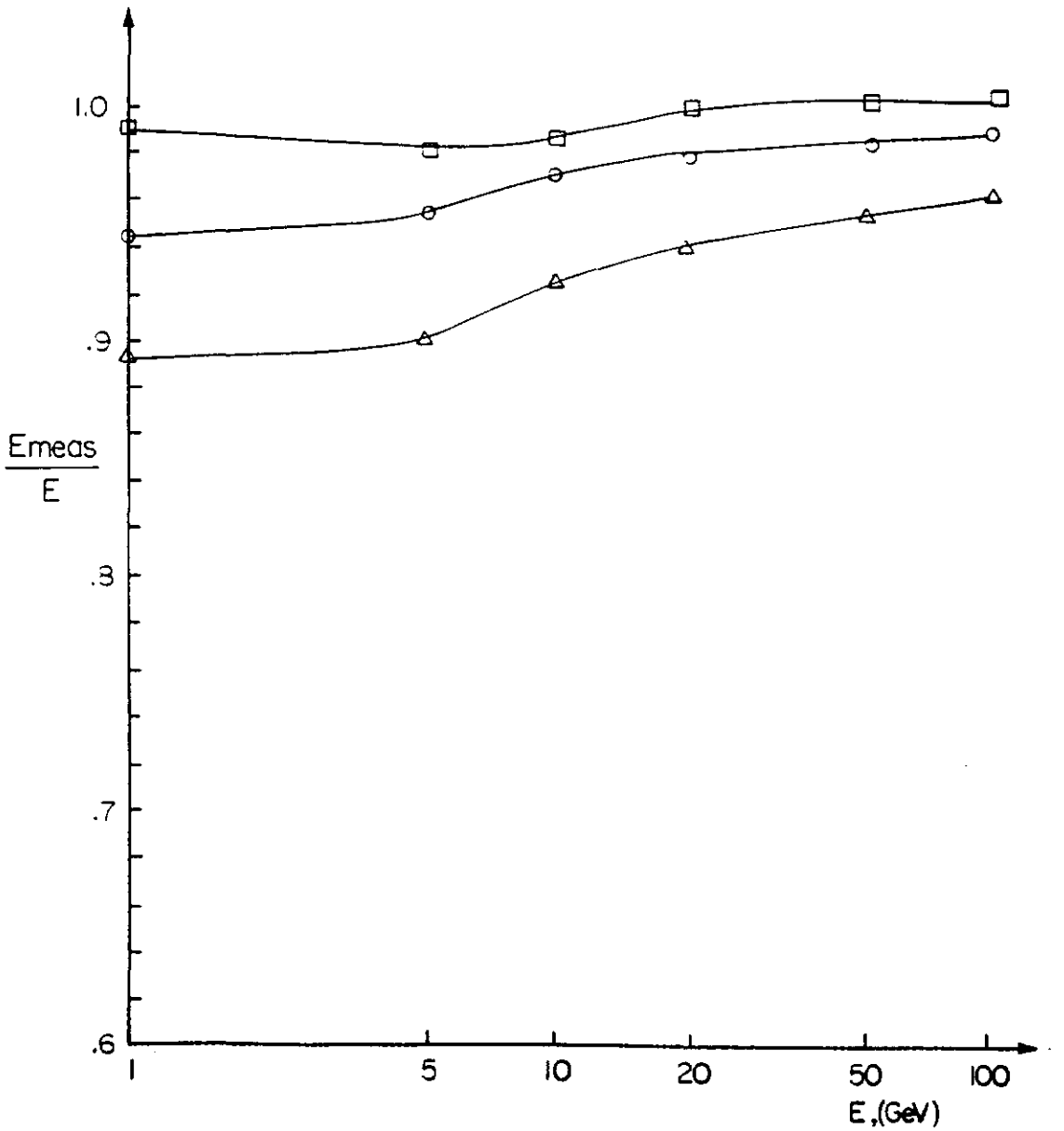

Figure 12.

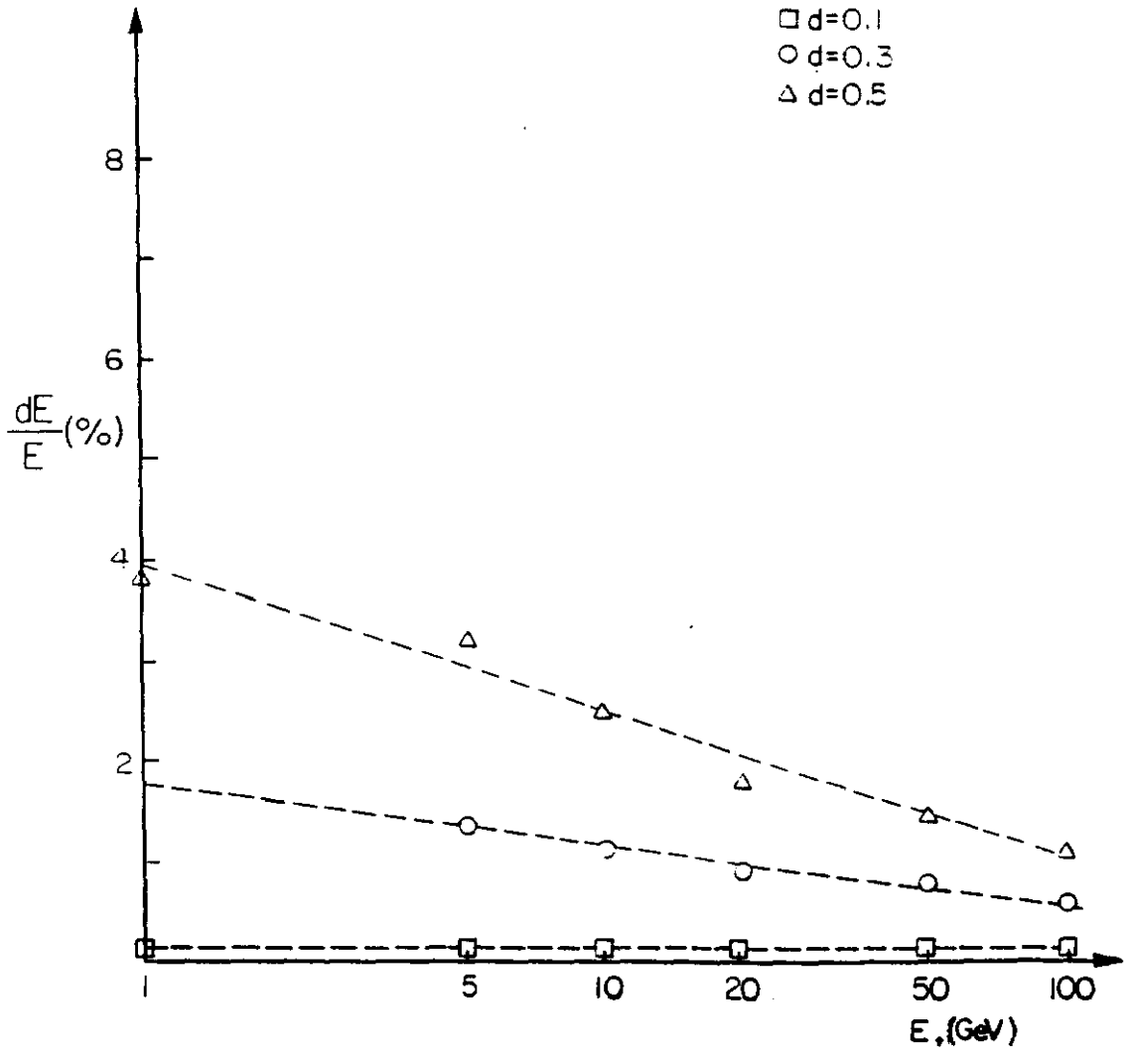

Figure 13.